Journal of Energy Storage 71 (2023) 107911

Contents lists available at ScienceDirect

Journal of Energy Storage

journal homepage: www.elsevier.com/locate/est

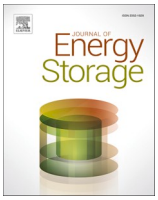

Research papers

Dynamic discharging performance of a latent heat thermal energy storage system based on a PID controller

Zhaoli Zhang [a,*], Jiayu Liu [a], Nan Zhang [a], Xiaoling Cao [a], Yanping Yuan [a], Muhammad Sultan [b], Shady Attia [c]

[a] School of Mechanical Engineering, Southwest Jiaotong University, Chengdu 610031, China
[b] Department of Agricultural Engineering, Bahauddin Zakariya University, Multan 60800, Pakistan
[c] Sustainable Building Design Lab, Dept. UEE, Faculty of Applied Sciences, University of Liège, Liège 4000, Belgium

ARTICLE INFO

Keywords:
Latent heat
PID control
Feedback control
Discharging performance
Parameter analysis

ABSTRACT

A PID controller is introduced into a latent heat thermal energy storage unit to compose a coupling system in order to control the discharging performance. Outlet temperature of the working fluid can be precisely regulated by means of its inlet velocity variation based on the PID controller. The theoretical model is built through combining heat transfer of the latent heat thermal energy storage unit with the PID controller. Experimental results are used to validate the proposed theoretical model. PID control analysis indicates that its parameters have obvious effects on performance of the coupling system. K_p of −0.02 m/(s·K), K_i of −0.15 m/(s^2·K) and K_d of −0.001 m/K are further optimized according to dynamic response of the transient outlet water temperature. System parameter analysis exhibits that higher target temperature produces larger heat discharging rate, which then reduces the outlet water flow rate accordingly. The discharging rate and total discharging energy of the latent heat thermal energy storage unit decrease with augment of the target outlet temperature. Increase of PCM melting point, thermal conductivity and latent heat is favorable of elevating the working fluid velocity. The discharging rate is improved by the PCM melting point, thermal conductivity and latent heat. The latent heat thermal energy storage units can separately obtain maximum discharging rates of 257.691, 294.437 and 257.603 W at 200 min for PCM melting point of 327.15 K, PCM thermal conductivity of 0.8 W/(m·K) and PCM latent heat of 250 J/g. It is apparent that PCM melting point, thermal conductivity and latent heat are conducive to enhancing the total discharging energy. The largest discharging energy at 200 min is respectively determined as 1280.409, 1060.105 and 974.153 kJ. Temperature and phase change contours can also be substantially affected by the system parameters. In conclusion, the built coupling system is beneficial to efficiently regulate and control discharging performance of latent heat thermal energy storage units.

1. Introduction

Energy crisis has increasingly involved into a great challenge to the sustainable social development [1,2]. Traditional energy still comes from combustion of limited fossil fuels consisting of coal, oil and gas, etc. The by-products during the combustion of fossil fuels cause serious environmental problems [3]. Feasible strategies are urgently needed to deal with the energy and environmental issues. Thermal energy is the most common form of energy and can be used in industrial production, building heating/cooling and district heating, accounting for over 50 % of the global terminal energy consumption [4]. Its rational and efficient utilization is critical to balance the energy structure system and realize net-zero emission of buildings. However, the utilization of thermal energy is largely confined by many factors, such as the time and space, etc.

Energy storage technology enables to store excess thermal energy in the short or long term and then release it under energy shortage occasions, achieving the purpose of energy reasonable dispatch [5,6]. Thermal energy storage is favorable of zero carbon emissions through two mechanisms: Cooperation with renewable energy and optimization thermal energy utilization rate. Theoretically, thermal energy storage can be classified into three categories: sensible heat, latent heat and chemical heat [7,8]. Among them, latent heat thermal energy storage (LHTES) is accomplished through the heat effect during phase transition of the phase change material (PCM) [9,10]. Compared to the sensible

* Corresponding author.
E-mail address: zzlyzhang@outlook.com (Z. Zhang).

https://doi.org/10.1016/j.est.2023.107911
Received 21 March 2023; Received in revised form 8 May 2023; Accepted 2 June 2023
Available online 23 June 2023

heat and chemical heat thermal energy storage, LHTES enables to charge more thermal energy at near constant temperature. Featured with the high thermal energy storage density and almost isothermal phase transition, LHTES has significant application potential in technological and engineering fields [11,12]. Several studies associated with the LHTES have been conducted from aspects of experiments and simulation.

Berardi et al. [13] added thin PCM layers to highly glazed apartments to stabilize indoor temperature. Experimental test found that integrating PCMs with different melting temperatures was effective in climates with large yearly temperature fluctuations. The PCM solidification period was confined by its poor thermal conductivity. Atinafu et al. [14] then fabricated hybrid materials based on biochar derived from bamboo and multiwalled carbon nanotubes to enhance PCM thermal conductivity. The hybrid material provided favorable morphological and interconnected framework structures for PCM encapsulation and energy storage capacity. Ishak et al. [15] synthesized LA/SiO_2 phase change microcapsule by the sol-gel method. Results confirmed that the proper microencapsulation of LA with SiO_2 shell had excellent thermal stability. Core-shell ratios played a vital role on the overall performance of microencapsulation. Guo et al. [16] designed LHTES units with angled metal fins used to solve the intermittency in time and space for solar energy systems. Results demonstrated that melting rates were improved for the angled-fin cases. Hosseinzadeh et al. [17] added nanoparticles into the star shape triplex LHTES system with internal fins to strengthen the thermal conductivity. They found a substantial improvement by using each technique individually, while the lowest solidification rate was assigned to the combination usage of both techniques. Lei et al. [18] improved the heat transfer performance of a LHTES by means of embedding metal foams into PCMs. The non-thermal-equilibrium energy model was applied in the numerical investigation. Results indicated that incorporation of copper foams into PCM significantly increased heat transfer performance of the LHTES. Liu et al. [19] achieved a high thermal conductivity and energy density compatible LHTES via porous AlN ceramic-based phase change composites. Further decorating AlN skeletons with TiN nanoparticles could significantly increase the solar absorptance, enabling proposed composites to be applicable for direct solar energy storage.

Based on the above review, it is obtained that PCM has excellent thermal physical properties, which could demonstrate incomparable technical advantages in energy storage and thermal management fields. Previous studies find that low thermal conductivity of PCM limits its popularization and application. Available strategies to enhance the PCM thermal conduction mainly include: metal fins, carbon materials, nanoparticles, microencapsulation, porous medium and external force field, etc. [20,21]. These findings verify that selected strategies are capable of improving PCM thermal diffusivity, indicating a great promotion to the LHTES.

Noticeably, it is perceived that discharging index of a LHTES system is critical to evaluate the system performance. Conventional studies are generally conducted by focusing on the discharging temperature variation at fixed flowing rate of the heat transfer fluid [16,22]. Few researches are involved in flowing rate variation of the heat transfer fluid while the discharging temperature is fixed in advance. Since the discharging process of a LHTES is a dynamic process, feedback is a powerful idea which could bring to revolutionary consequence with drastic improvement to the dynamic control [23]. The Proportional-Integral-Derivative (PID) controller is by far the most dominating feedback form. Most of the control systems that are implemented with utilization of the PID controller because of its simple structure, ease implementation and mature technology.

Ajour et al. [24] installed a new PID controller to adjust interior temperature compatible with the PCM melting range. Several different PCMs were added to the wall with the intention of forecasting the energy demand from a green building. Effect of PCM thickness and type on energy saving were analyzed in their research. Alghamdi et al. [25] designed a PID controller in the air conditioner to regulate the hot/cold fluid flow in hot/cold coils, in order to lower maintenance, energy consumption and initial costs. The thermodynamic analysis of an air handling unit was investigated. Simulation results showed that the air handling unit could provide suitable thermodynamic conditions in the interior space (T = 295.15 K and RH = 55 %). Piao et al. [26] established a compartment physical model of an electric car to simulate the heating process of the heat pump air conditioning system. A fuzzy PID is proposed to control the temperature of the passenger compartment. Thermal comfort of the passenger cabin was evaluated through a thermal comfort model of cabin temperature and humidity. Su et al. [23] configured a parameter self-tuning PID control approach to improve reliability of the greenhouse climate control. Four PID controllers were brought to generate the control signals of heating, fogging, CO_2 injecting and ventilation. Experimental results indicated the effectiveness proposed method has good applicability and generality. Ma et al. [27] reported a new flue gas waste heat recovery system with its control strategy proposed of the intelligent control technology and the principle of phase-change heat transfer. Control strategies of the new system were designed to control the outlet flue gas temperature and system pressure. Their paper could provide a theoretical basis for improving control performance of the new proposed system. Huo et al. [28] brought a PID controller to a hybrid solar-fossil fuel power generation and storage, in order to investigate the dynamic characteristics and real-time control. The control performance indexes were improved by 66.7 % on average. The controller was confirmed to be a better control method for dynamic operation of the HFSS-PGS system.

It is rationally concluded that the PID controller has excellent robustness and high reliability, enabling to address the parameter and model uncertainties in practice. However, few studies associated with the PID controller applied in the LHTES. It is noteworthy to deeply explore integration of a PID controller with the LHTES system and the synergy operating mechanism of them subjected to a target outlet temperature. This paper puts forward a novel LHTES model and its dynamically control strategy is established based on the coupling of the PID control and phase change heat transfer. Parameters of the PID controller are firstly optimized in the built coupling model. Effect of target outlet temperature and thermophysical properties (melting point, thermal conductivity and latent heat) of PCM on discharging performance of the built coupling model are also revealed in this investigation.

2. Methodology

2.1. Physical model of LHTES

The most common LHTES system is designed as a three-dimensional rectangular structure as indicated in Fig. 1. It is illustrated in Fig. 1 (a) that several metal pipes are placed evenly along vertical direction of the rectangular phase change system, allowing a working fluid passing through them to extract thermal energy. This paper adopts water as the working fluid owing to its superior heat transfer capacity, which is the most commonly used working media in numerous application fields. A separator and a collector are separately installed at the inlet and outlet to ensure that the fluid is uniform in each pipe. In order to deal with the inherent thermal conductivity deficiency of PCM, many round copper fins are practically mounted on the water pipes. Thermal energy stored in the phase change system can be rapidly released through the heat transfer enhancement of copper fins. It is validated that the solid-liquid PCM inevitably suffers from liquid leakage after phase transition. To address this limitation, this paper prefers to select a form-stable PCM prepared based on an available shaping method [29–31]. Thus, PCM enables to maintain the steady shape even when it completely transforms into liquid. Fig. 1 lists detailed thermophysical properties of the utilized PCM and copper. Considering height of the phase change system is far larger than its width or length, heat transfer in the height direction hardly affects that in width or length direction. The entire rectangular phase change system is simplified into a narrow part including only one

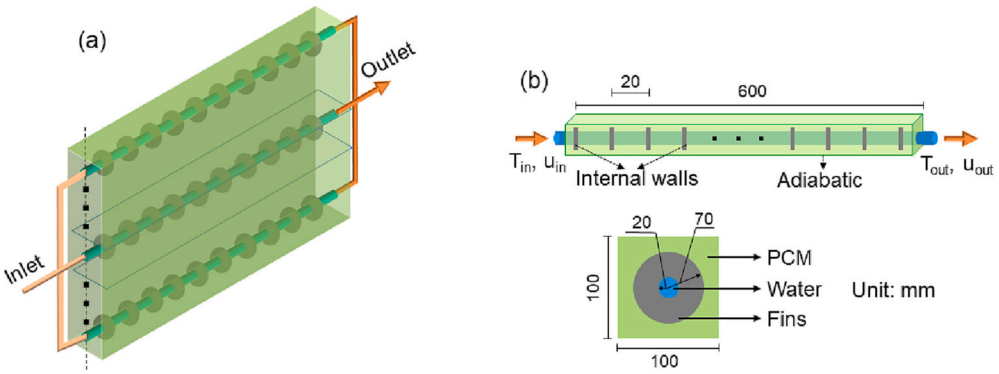

Fig. 1. Configurational schematic of the LHTES system. (a) System configuration, (b) Physical model.

water pipe. It is specific in Fig. 1 (b) that length of the physical model is 600 mm. The cross-section is assumed as square with related side length of 100 mm. The radius of copper pipes and fins are fixed as 20 and 70 mm, respectively. Table 1 (b) shows that the interval between two adjacent copper fins is 20 mm.

2.2. Governing eqs.

2.2.1. PCM

Theoretical calculation of the LHTES can be rationally simplified according to several feasible assumptions as listed in the follows [6,32,33]:

(1) PCM is regarded as the form-stable material without considering liquid flow.
(2) Thermophysical properties of solid and liquid PCM are different.
(3) Local thermal non-equilibrium exists between the working fluid and PCM.

This paper aims to evaluate dynamic discharging performance of the LHTES system. It is obvious that PCM incorporated in the phase change system undertakes solid-liquid phase transition that enables to release enormous thermal energy during the investigation. An enthalpy-porosity method is adopted to account for the phase change heat transfer of PCM [22]. Theoretically, the whole computational domain (Fig. 1) is termed as a 'pseudo' porous zone. The related porosity of each cell can be characterized by liquid fraction (f). Based on the above assumption, the governing equations of PCM in terms of energy conservation are listed in Eqs. (1)–(3).

$$\frac{\partial(\rho_m H)}{\partial \tau} = \nabla(\lambda_m \nabla T) + S_{r,m} \tag{1}$$

$$H = h_s + fL \tag{2}$$

$$h_s = h_{ref} + \int_{T_{ref}}^{T} c_{p,m} dT \tag{3}$$

where τ is the time; ρ_m, λ_m and $c_{p,m}$ are the density, thermal conductivity and specific heat of PCM; H, h_s and L denote the enthalpy, sensible heat and latent heat of PCM; h_{ref} and T_{ref} stand for the reference enthalpy and temperature; $S_{r,m}$ represents the source term of PCM energy conservation equation and is numerically equivalent to $-S_{r,f}$ in water energy conservation equation.

The volume proportion of liquid PCM is determined by the liquid fraction during the research. That is to say, $f = 0$ or 1 respectively represents PCM is completely in solid or liquid state. The f will be linearly changed within the range of 0 to 1 during the mushy region between solid and liquid when PCM is subjected to the working fluid [9]. The formula to calculate f is expressed in Eq. (4).

$$f = \begin{cases} 0, T < T_{m1} \\ \dfrac{T - T_{m1}}{T_{m2} - T_{m1}}, T_{m1} < T < T_{m2} \\ 1, T > T_{m2} \end{cases} \tag{4}$$

where T_{m1} and T_{m2} are the initial and terminal temperatures of PCM during the melting zone; T is the transient temperature of PCM.

2.2.2. Working fluid

Water is employed as the working fluid passing through the phase change system with the purpose of extracting thermal energy to satisfy demand from available fields. Thermal energy discharging rate is largely dependent to the water velocity. Lower water velocity is selected in this study in order to accelerate the heat release rate. The flowing condition is treated as laminar flow on account of low Re. The corresponding governing equations of water from the perspectives of continuity, momentum and energy conservation are expressed as follows [22,33].

$$\frac{\partial(\rho_f)}{\partial \tau} + \nabla(\rho_f \vec{u}) = 0 \tag{5}$$

$$\frac{\partial(\rho_f \vec{u})}{\partial \tau} + \nabla(\rho_f \vec{u}\vec{u}) = -\nabla p + \mu_f \nabla^2 u + S_{u,f} \tag{6}$$

$$\frac{\partial(\rho_f c_{p,f} T)}{\partial \tau} + \nabla(\rho_f \vec{u} c_{p,f} T) = \nabla(\lambda_f \nabla T) + S_{r,f} \tag{7}$$

where ρ_f, λ_f and $c_{p,f}$ are the density, thermal conductivity and specific heat of water; u, p and T denote velocity, pressure and temperature of water, respectively; $S_{u,f}$ and $S_{r,f}$ represent the source terms in momentum and energy conservation equations.

Table 1
Thermophysical properties of PCM and copper.

Properties	PCM	Copper
Density (kg/m^3)	950(s)/920(l)	8960
Thermal conductivity (W/(m·K))	0.2	400
Specific heat (J/(kg·K))	2050(s)/2250(l)	385
Melting point (K)	321.65(s)/316.65(l)	–
Latent heat (kJ/kg)	198	–
Thickness (m)	–	0.002

2.3. PID control

PID control is one of the earliest developed control strategies and it can be widely found in practical engineering applications. A PID controller generally refers to an algorithm that has been developed for many years. It has increasingly become a mature industrial control because of its simple structure, reliable operation and convenient

adjustment. Application of the PID control is of particular convenience in occasions where the structure and parameters of the controlled object are hardly mastered, or the precise mathematical model is difficult to obtained, or other available control technologies are missing. In other words, the PID control technology is suitable for the controlled object that is poorly regulated through effective measurement methods. A PID controller is usually conducted based on the system error, using proportion, integration and differentiation to calculate quantity of the controlled object. Three related characteristic parameters are referred as the proportional gain (K_p), integral gain (K_i) and differential gain (K_d), respectively. This paper would like to control the outlet water temperature by means of changing the water flowing rate as indicated in Fig. 2. A feasible outlet water temperature is initially set in the phase change system. The corresponding water flow rate is then calculated through the PID control as shown in Eqs. (8)–(9). It is noticeable that the water flow rate is closely related to the outlet water temperature, demonstrating timely and accurate control applied in discharging process of the phase change system.

$$u_{in}(\tau) = K_p T_e(\tau) + K_i \int_0^{\tau} (T_e(\tau))d\tau + K_d \frac{dT_e(\tau)}{d\tau} \tag{8}$$

$$T_e(\tau) = T_{set}(\tau) - T_{pv}(\tau) \tag{9}$$

where K_p, K_i and K_d are three parameters of the PID controller; $T_e(\tau)$ is temperature difference between the set target outlet water temperature ($T_{set}(\tau)$) and transient outlet water temperature ($T_{pv}(\tau)$).

2.4. Discharging performance

2.4.1. Discharging rate

Transient discharging rate can reflect thermal energy extracting rate from a LHTES system. Theoretically, transient discharging rate of the novel coupling system is corresponding to enthalpy change of the working fluid experiencing the LHTES system. The related calculation formula is listed in Eq. (10).

$$\dot{q}(\tau) = c_{pf}\dot{m}(\tau)\left(T_{pv}(\tau) - T_0\right) \tag{10}$$

where $\dot{m}(\tau)$ denotes the transient mass flow rate of the working fluid; T_0 represents the fluid inlet temperature.

2.4.2. Total discharging energy

The LHTES system is capable of continuously discharging thermal energy as long as the working fluid temperature is lower than that of PCM. The accumulated thermal energy increases with elapse of time. Total discharging energy can be determined based on the discharging rate as shown in Eq. (11).

$$Q(\tau) = \int_0^{\tau} \dot{q}(\tau)d\tau \tag{11}$$

2.5. Initial and boundary conditions

2.5.1. Initial condition

The object of this paper is to evaluate discharging performance of the LHTES system. Thus, the phase change system is initially designed as full charged and related temperature is 5 K higher than the PCM melting point. The copper pipes and fins have identical initial temperature to that of PCM. As for the working fluid, water is assumed to pass through these copper pipes at the inlet temperature of 293.15 K, aiming to extract thermal energy from the LHTES system.

2.5.2. Boundary condition

Boundary condition of the theoretical model should be stated prior to the investigation. It is illustrated in Fig. 1 (b) that only part of the phase change system is considered in the numerical simulation. Surroundings of the physical model are termed as adiabatic without heat losing. The left boundary belongs to the inlet of water in the flowing field, while it flows out of the phase change system from the right boundary. The copper pipes and fins are treated as thin layers in the temperature field.

2.6. Model solving and validation

2.6.1. Model solving

Governing equations of continuity, momentum and energy conservation over the computational region are firstly discretized through the staggered grid technology. The unstructured grid consisting of triangular element is adopted in this calculation. COMSOL Multiphysics based on the finite element method is utilized to solve three governing equations, on account of its inherent capacity to implement adaptive remeshing. Calculation time step is charged within a rational order by a free backward differentiation formula. A parallel direct solver with a rational residual error is about to solve the residual equations. Relative residual of 10^{-4} is checked for continuity, momentum and energy conservation equations at each time step of the numerical calculation in order to maintain a highly accurate resolution.

2.6.2. Independence

The mesh number is reckoned as a crucial parameter to the finite element method. Its independency is thus discussed in detail before conducting the numerical investigation. Four mesh numbers of 4650, 6660, 10,800 and 12,520 are separately checked in independency analysis of the numerical model with the results plotted in Fig. 3. The phase change system is started at the initial temperature of 329.15 K, whereas the inlet water temperature is fixed at 293.15 K. A PID controller is conducted under the K_p of −0.02 m/(s·K), K_i of −0.15 m/(s^2·K) and K_d of −0.001 m/K, respectively. Outlet water temperature and velocity from the phase change system as function of time are detected. It is perceived in Fig. 3 that there exist significant fluctuations in terms outlet water temperature and velocity owing to dynamic regulation of the PID controller. The transient outlet water temperature and velocity are nearly overlapped when the mesh number is larger than 10,800. Results almost maintain constant with continuous augment of

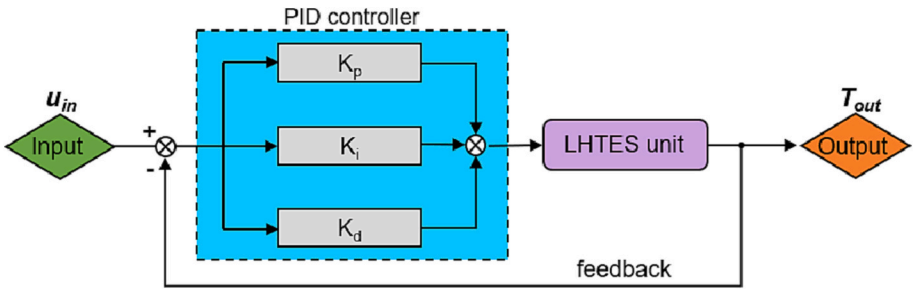

Fig. 2. Operating principle of the LHTES system coupled with a PID controller.

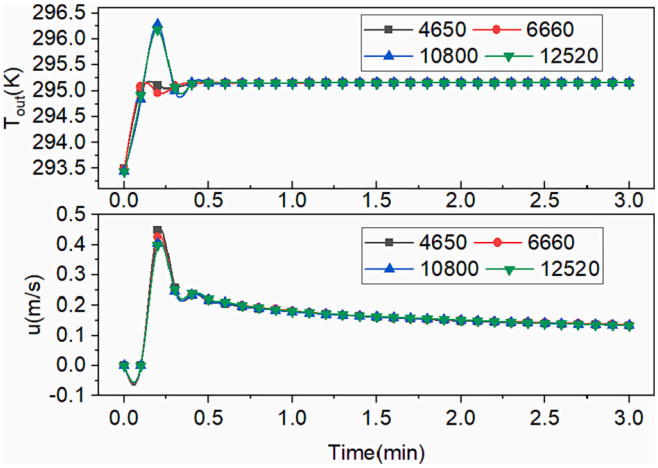

Fig. 3. Mesh independence of the built numerical model.

mesh number. Whereas, the corresponding calculated period will become much longer under the condition of larger mesh number. Therefore, the mesh number of 10,800 is adopted in the following research, taking both computational accuracy and saving costs into consideration.

2.6.3. Model validation

The numerical model of LHTES system is verified through comparison between calculated results of the built numerical model and the corresponding phase change experiment. It is displayed in Fig. 4 that the phase change unit belongs to a concentric tube structure having inner and outer diameters of 15 mm and 60 mm, respectively. The entire length of the phase change unit is 800 mm. 5 mm transparent plexiglass is covered on outside of the phase change unit to guarantee thermal insulation. A form-stable PCM is filled in the interval between inner and outer tubes. This paper selects water as the heat transfer fluid flowing through the inner tube. Experimental principle, setup and comparable results are indicated in Fig. 4 (c). The suitable velocity and temperature of inlet water (0.005 m/s and 333.15 K) are adopted in PCM melting process analysis. Whereas, the PCM solidification analysis employs low-temperature inlet water (0.005 m/s and 303.15 K). It is illustrated in Fig. 4 that calculated outlet water temperature is in excellent accordance with experimental result with elapse of time. Difference between the real object and assumed physical model might attribute to slight discrepancy between calculated and experimental results. Thus, it is rationally inferred that the built numerical model is accurate enough to be utilized in the following research.

3. Results and discussion

3.1. PID control analysis

The PID control analysis is carried out at the water inlet temperature of 293.15 K. Considering the configuration of LHTES system is tiny, a low temperature rise of 2 K between water outlet and inlet temperatures is adopted in this part. Indeed, K_p, K_i and K_d are three parameters that can produce practical effect on performance of a PID control. The PID control commissioning is divided into three steps: (1) K_p parameter determination, (2) K_i parameter determination under constant K_p and (3) K_d parameter determination under constant K_p and K_i.

3.1.1. K_p parameter

Transient outlet temperature of water varied with K_p is indicated in Fig. 5, when K_i and K_d are assumed as 0. It is found that the water outlet temperature increases firstly and then decreases noticeably as the time elapses at all cases. This sight is attributed to K_p introduction into the PID control of the phase change system. As K_p is a proportional coefficient, increasing K_p will accelerate response of the coupling system, which is able to speed up the output value. Fig. 5 shows that the maximum temperature of outlet water rises with the augment of K_p, arriving 296.02, 296.20, 296.36, 296.45, 296.64, 297.00, 297.42 and

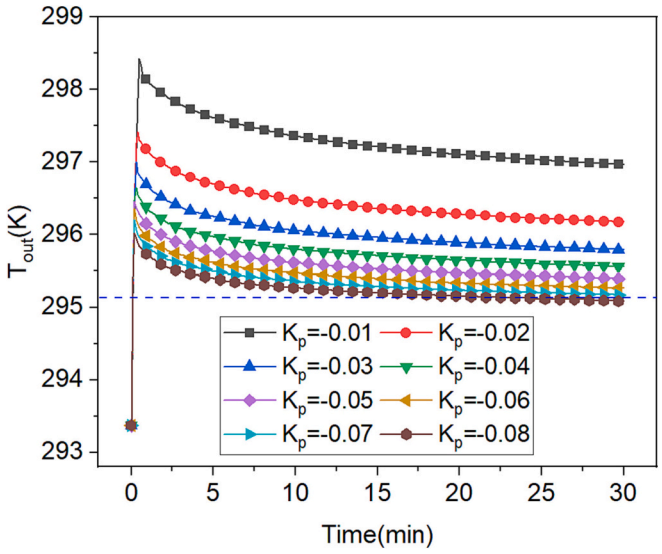

Fig. 5. Transient outlet water temperature of the LHTES unit varied with K_p (K_i = 0, K_d = 0).

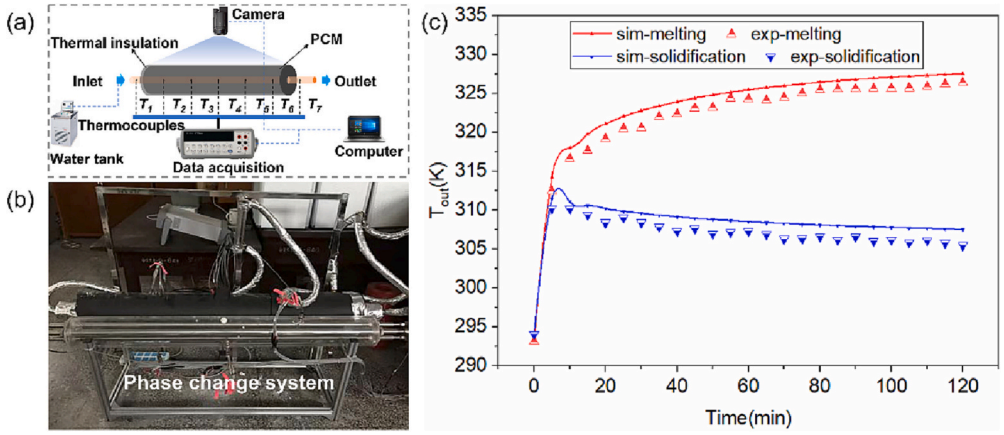

Fig. 4. Experimental validation of the built numerical model. (a) Experimental principle, (b) Experimental setup; (c) Comparable results.

297.88 K, respectively. Whereas, larger proportional coefficient enables to cause more significant overshoot and oscillation of the coupling system. The initial water outlet temperature is determined as 296.96 K and drops to 295.09 K when the K_p continuously decreases from −0.01 to −0.08 m/(s·K). Compared to the maximum temperature of outlet water, it is perceived that variations of the water outlet temperature are individually 0.92, 1.25, 1.21, 1.08, 1.06, 1.04, 1.03 and 0.93 K. Thus, this study preliminarily selects three K_p (−0.02, −0.03 and −0.04 m/(s·K)) in the following research.

3.1.2. K_i parameter

Fig. 6 plots the transient outlet water temperature as function of K_i. It is exhibited that outlet water temperature fluctuates slightly when the K_i is introduced into the phase change system. As the time elapses, water outlet temperature continuously approaches to the target temperature (295.15 K). It is known that single K_p adjustment hardly eliminates error between the controlled and the given outlet temperatures. There must exist a stable error to maintain a valid output and keep the water outlet temperature reliable. Since the output of a PID controller is proportional to the integral of the input error signal, K_i is designed to eliminate the static error and improve error-free degree of the phase change system. The strength of the integral action is dependent on the magnitude of constant K_i. A larger K_i generally induces a weaker integral action. Therefore, it is obtained in Fig. 6 (a) that fluctuation of water outlet temperature reduces with the growth of K_i. The minimum temperature variation of outlet water is calculated as 0.42 K at the K_i of −0.15 m/(s^2·K). Similarly, Fig. 6 (b)–(c) present that temperature variation of outlet water decreases to merely 0.07 and 0.05 K when K_i of −0.15 m/(s^2·K) is employed in the two PID controllers (K_p = −0.03 and − 0.04 m/(s·K)). It is further appeared that outlet water temperature variation frequency at K_i of −0.15 m/(s^2·K) is lest compared to other K_i cases. Comparable results verify that K_i of −0.15 m/(s^2·K) causes lowest fluctuation in terms of outlet water temperature, releasing outstanding effect on dynamic control of the LHTES system.

3.1.3. K_d parameter

K_d reflects the change trend of the deviation signal, which can introduce an effective early correction signal into the PID control before the deviation signal becomes too large. K_d is thus conducive to accelerating the system action speed and reducing the adjustment time. Fig. 7 shows that outlet water temperature changed with K_d. It is exhibited that its fluctuation decreases sharply as the K_d rises in any K_d case. The output of the controller is proportional to differential of the input error signal. A Larger K_d brings to a stronger differential action, inducing lower fluctuation in terms of outlet water temperature. It is determined in Fig. 7 (a) that the temperature fluctuation of outlet water in the coupling systems with K_d of −0.1 m/K is 0.23 K, declining to 0.17, 0.13 and 0.12 K for K_d cases of −0.05, −0.01 and −0.0001 m/K, respectively. Compared to the outlet water temperature variation in Fig. 6, it is specific that less outlet water temperature variation frequency occurs in Fig. 7 owing to the K_d function. Thus, K_d of −0.001 m/K is further selected to be utilized in PID control of the phase change system based on the K_p and K_i optimization in above section.

3.2. Target outlet temperature analysis

Fig. 8 elaborates the transient discharging performance of the LHTES system as function of the target outlet temperature. It is revealed that outlet water temperature sharply reaches target temperature after fluctuation in a short time, meaning that the PID controller is a preferable strategy to make outlet water temperature close to the target temperature. Fig. 8 (a) show that the outlet water temperature can be well maintained at target temperature even at 200 min. The flow rates of outlet water running out of the phase change system at various target temperatures are presented in Fig. 8 (b). It is found that the outlet water flow rate reduces obviously with the elapse of time, as results of thermal energy released from the phase change system. It is perceived that decrease of the water flow rate is caused by the increase of target temperature under the same heat exchange condition. That is to say, higher target temperature produces larger heat discharging rate, which then reduces the outlet water flow rate accordingly. Specially, the available operating period of phase change system is tested as 128.8 min and then drops to 24.6, 3.3 and 0.7 min, taking the water flowing rate of 0.2 m/s as the objective. When the water flowing rate drops to 0.1 m/s, Fig. 8 (b) proves that the available operating period becomes larger in comparison to that at the higher flowing rate case. It is reported that water can operate stably approximately 123.5, 45.7 and 10.4 min under the target outlet temperatures of 294.15–295.15 K.

The discharging rate of latent heat thermal energy storage is presented in Fig. 8 (c) and it is discovered that lower target outlet temperature means less heat transfer temperature difference between PCM and the working fluid, indicating larger discharging rate compared to the higher target outlet temperature cases. With the elapse of time, the discharging rate of latent heat thermal energy storage system decreases gradually and finally arrives at 257.691, 233.894, 217.419 and 208.572 W at 200 min. Fig. 8 (d) reveals the released thermal energy of various latent heat thermal energy storage units. It is found that total discharging energy increases significantly as the time elapses. This sight is due to the fact that the heat exchange between PCM and the heat transfer fluid continues as long as there is temperature difference between them. Whereas, the total discharging energy decreases with the augment of the target outlet temperature. At 200 min, the total discharging energy is individually calculated as 1280.409, 1114.910, 1004.443 and 918.373 kJ. The temperature and phase change contours are shown in Fig. 8 (e) and (f). Related results exhibit that stored thermal energy is released to the heat transfer fluid during the discharging process, producing darker color in terms of temperature and phase change contours at lower target outlet temperature.

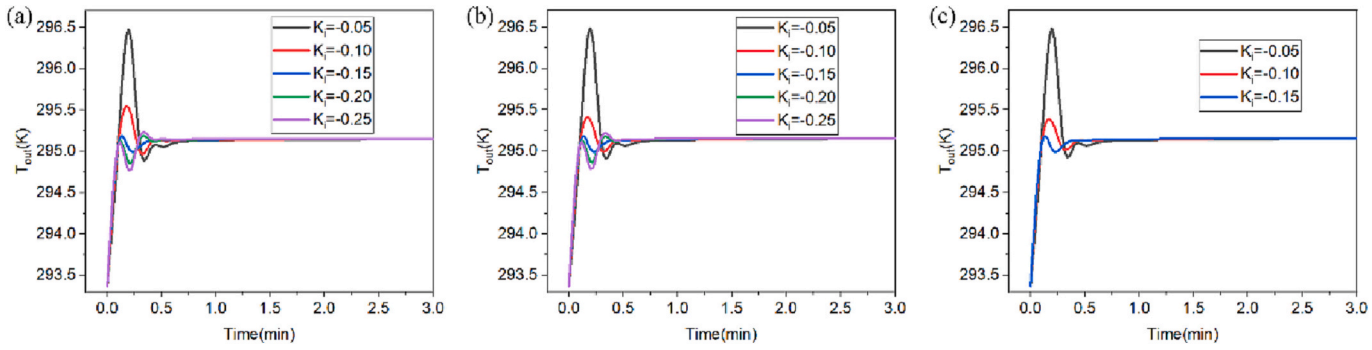

Fig. 6. Transient outlet water temperature of the LHTES unit varied with K_i. (a) K_p = −0.02 m/(s·K), K_d = 0; (b) K_p = −0.03 m/(s·K), K_d = 0; (c) K_p = −0.04 m/(s·K), K_d = 0.

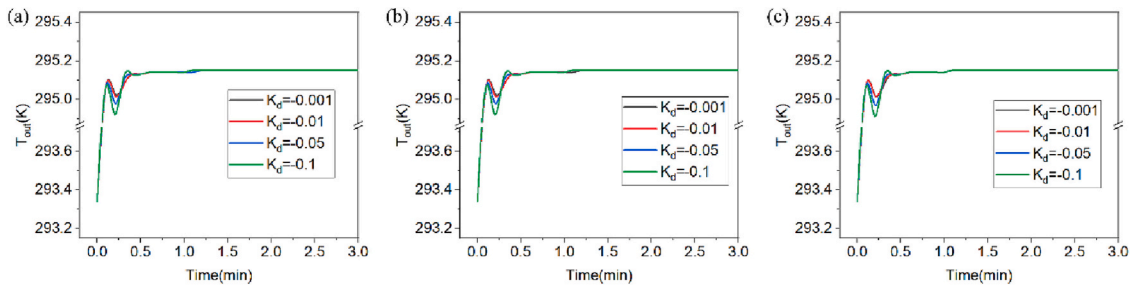

Fig. 7. Transient outlet water temperature of the LHTES unit varied with K_d. (a) $K_p = -0.02$ m/(s·K), $K_i = -0.15$ m/(s^2·K); (b) $K_p = -0.03$ m/(s·K), $K_i = -0.15$ m/(s^2·K); (c) $K_p = -0.04$ m/(s·K), $K_i = -0.15$ m/(s^2·K).

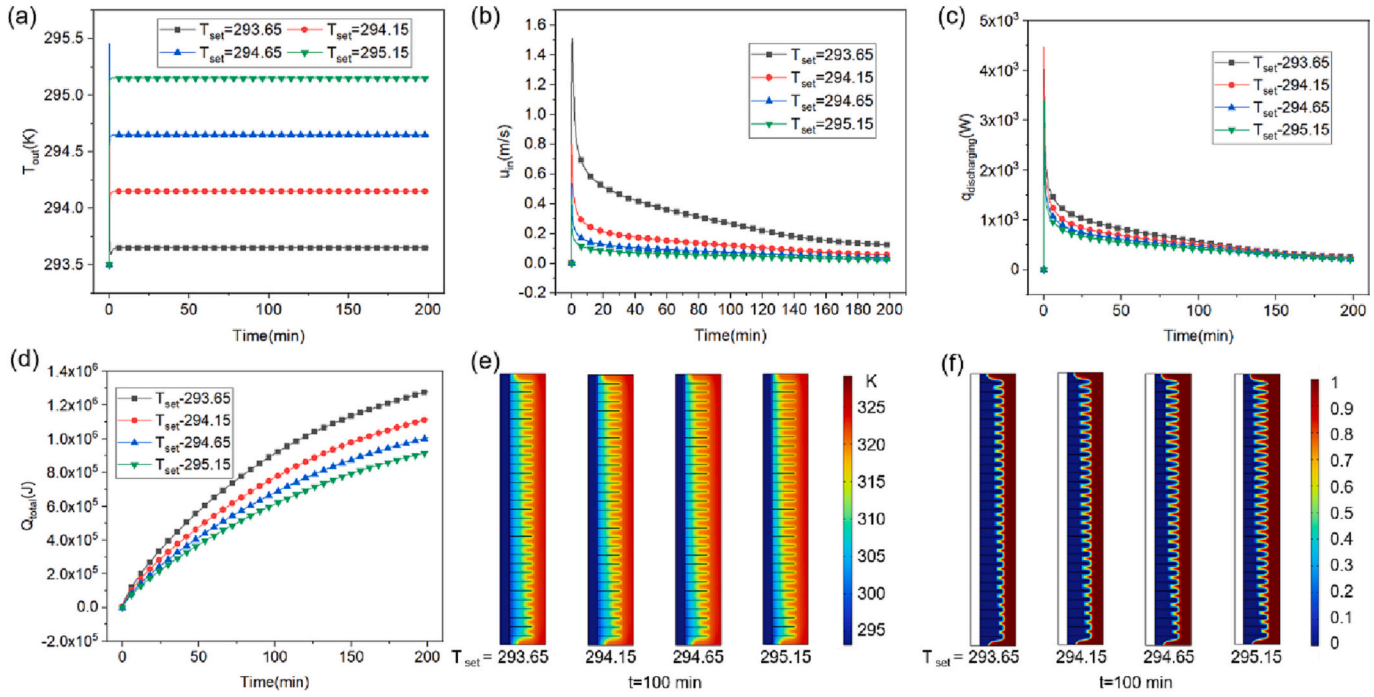

Fig. 8. Transient discharging performance of the LHTES system with various target outlet temperatures. (a) Outlet water temperature, (b) Outlet water flow rate, (c) Discharging rate, (d) Total discharging energy, (e) Temperature contour and (f) Phase change contour.

3.3. PCM thermoptometries analysis

3.3.1. Melting point of PCM

Discharging performance of the LHTES system with various PCM melting points is illustrated in Fig. 9. It is apparent that outlet water temperature has large fluctuation in the initial stage, which is resulted from function of the PID controller. The PID controller enables to induce the actual outlet water temperature to get closer to the target temperature with the time elapses, reaching well agreement with the target temperature in a short time. Fig. 9 (a) indicates that higher PCM melting point results in lower fluctuation in terms of outlet water temperature. Outlet water flow rate can be affected by the melting points of PCM encapsulated in the phase change system. It is clear that higher PCM melting point leads to more intense discharging performance and larger outlet water flow rate in this scenario. As time elapses, liquid PCM changes into solid with stored thermal energy being extracted from the phase change system. The outlet water flow rate variation caused by PCM melting points decreases with elapse of time. It is observed in Fig. 9 (b) that it takes 4.9 min for outlet water flow rate reducing to 0.1 m/s in the phase change system with PCM melting point of 315.15 K. The available operating period rises with augment of the PCM melting point, approaching 9.0, 16.1 and 26.9 min for the PCM melting point cases of 315.15–327.15 K. When outlet water flow rate is selected as 0.05 m/s, phase change system is capable of continuously working 61.0, 90.9, 106.8 and 112.5 min at the PCM melting points of 315.15–327.15 K.

Fig. 9 (c) illustrates the discharging rates of LHTES units at various PCM melting points. It is obvious that larger PCM melting point requires the phase change unit to operate at higher initial temperature in order to ensure the liquid PCM is fully loaded, leading to larger heat transfer temperature difference between PCM and the working fluid and higher discharging rate accordingly. The transient discharging rates drops as the time elapses, reaching almost a steady result of 200 W at 200 min. Considering larger PCM melting point causes higher discharging rate of the LHTES unit, it is thus perceived in Fig. 9 (d) that total discharging energy climbs as the PCM melting point rises. The total discharging energy increases while the amplify gradient decreases with the elapse of time, owing to the decline of heat transfer performance between PCM and the working fluid. It is specific that the total discharging energy is 775.515, 885.508, 954.005 and 1060.105 kJ for the LHTES units containing PCM with melting points of 315.15–327.15 K. Fig. 9 (e) and (f) denote the temperature and phase change contours of various LHTES units at 100 min. It is obtained that more significant temperature difference occurs in the phase change unit with higher PCM melting point, as result of PCM having higher initial temperature. The phase change

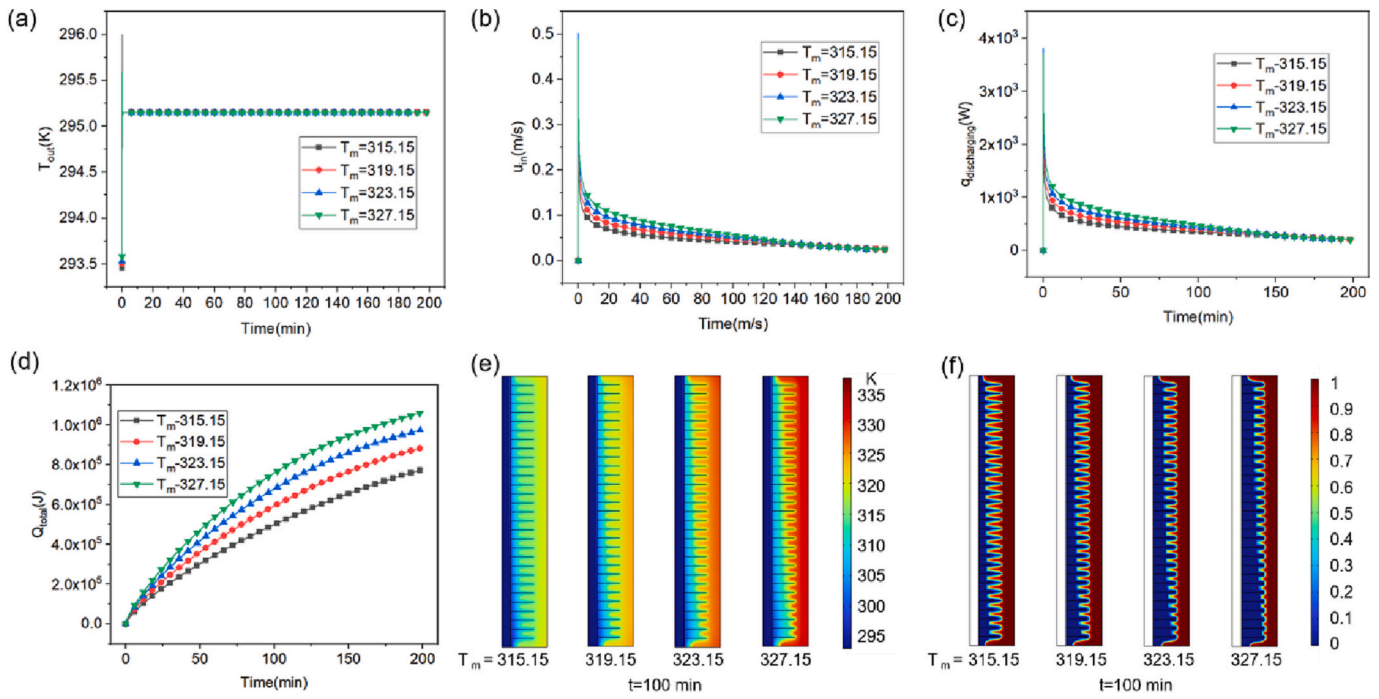

Fig. 9. Transient discharging performance of the LHTES system with various PCM melting points. (a) Outlet water temperature, (b) Outlet water flow rate, (c) Discharging rate, (d) Total discharging energy, (e) Temperature contour and (f) Phase change contour.

contour shows that PCM melts faster at higher PCM melting point case, implying more thermal energy can be extracted from the LHTES unit in this scenario.

3.3.2. *Thermal conductivity of PCM*

Considering PCM utilized in the phase change system is form-stable, its thermal conductivity can be affected by the shaping strategies, such as wrapping, porous medium, micro-encapsulation, composite spinning, etc. It is believed that PCM thermal conductivity can be greatly enhanced when being incorporated into a form-stable composite PCM. This paper assumes that a form-stable composite PCM is utilized in this study and discharging performance of the phase change system with various PCM thermal conductivity is evaluated. Obtained results in Fig. 10 (a) displays that outlet water temperatures of the phase change system quickly approach the target outlet temperature of 295.15 K, revealing the PID controller is beneficial to regulate the outlet water temperature. PCM thermal conductivity only exerts limited effect on the outlet water temperature in the initial stage. It is identified in Fig. 10 (b) that the outlet water flow rate climbs up to 0.44836, 0.41662, 0.43798 and 0.42315 m/s when discharging process of the phase change system suddenly starts. With elapse of time, it gradually decreases as result of the reduction of available thermal energy in the LHTES units that can be

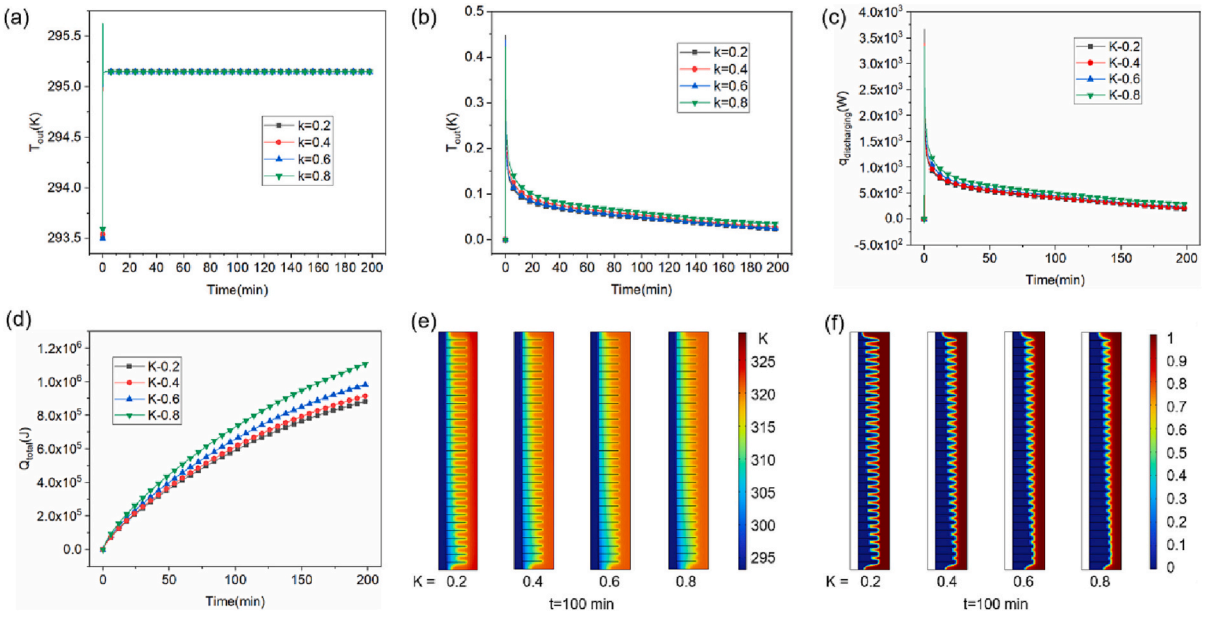

Fig. 10. Transient discharging performance of the LHTES system with various PCM thermal conductivity. (a) Outlet water temperature, (b) Outlet water flow rate, (c) Discharging rate, (d) Total discharging energy, (e) Temperature contour and (f) Phase change contour.

released. Fig. 10 (b) shows that outlet water flow rate at 200 min can drop as low as 0.02326, 0.02774, 0.02483 and 0.03505 m/s for the PCM thermal conductivity of 0.2, 0.4, 0.6 and 0.8 W/(m·K), respectively.

Discharging rate of the LHTES system with various PCM thermal conductivity is plotted in Fig. 10 (c). It is discovered that it decreases substantially with elapse of time, which is limited by the weakened heat transfer between PCM and the working fluid. Larger PCM thermal conductivity can bring to better heat diffusion, inducing faster discharging rate from the LHTES system. At 200 min, the discharging rate declines from 294.437 W to 195.358 W, when the PCM thermal conductivity decreases from 0.8 to 0.2 W/(m·K). Similarly, reduction of the discharging rate enables to lower the total discharging energy. Fig. 10 (d) indicates that the total discharging energy increases as the PCM thermal conductivity rises. It is determined that the total discharging energy can arrive to separately 1112.224, 987.189, 918.373 and 885.508 kJ for PCM thermal conductivity cases of 0.8, 0.6, 0.4 and 0.2 W/(m·K). Fig. 10 (e) shows that more uniform temperature distribution is appeared in temperature contour of the LHTES unit with larger PCM thermal conductivity, owing to improved heat transfer performance. It is illustrated in Fig. 10 (f) that higher PCM thermal conductivity is conducive to accelerating the solidification. Larger solidification zone can be found in phase change contour of the LHTES unit with higher PCM thermal conductivity. This sight is well corresponding to the variation of total discharging energy.

3.3.3. *Latent heat of PCM*

The PCM latent heat is a critical parameter to discharging performance of the LHTES system, as thermal energy is primarily stored in the form of latent heat. It is revealed in Fig. 11 (a) that obvious fluctuation of outlet water temperature is observed only in the initial stage. This result can be explained by dynamic regulation of the PID controller. Featured with simple algorithm, excellent robustness and high reliability, it has widely used in the industrial process control, especially for deterministic control systems to establish accurate mathematical models. Outlet water temperature of the phase change system quickly reaches the target temperature after a short-term fluctuation. Actually, the PCM latent heat hardly exerts influence on outlet water temperature. When it comes to the outlet water flow rate, Fig. 11 (b) illustrates that it sharply rises to 0.44452, 0.44869, 0.43798 and 0.44612 m/s owing to the outlet water temperature fluctuation under the PID control action. It is revealed that the outlet water flow rate reduces with elapse of time, which is attributed to discharging capacity attenuation of the phase change system. Higher PCM latent heat implies larger thermal energy stored in the phase change system, demonstrating slighter decline to the outlet water flow rate compared to the lower PCM latent heat case. It is specific that outlet water enables to work continuously until 55, 73.3, 98.7 and 108.7 min for phase change system with PCM latent heat of 100–250 kJ/kg, when the minimum outlet water flow rate is fixed at 0.05 m/s.

It is presented in Fig. 11(c) that the discharging rate changes limited with the PCM latent heat variation in the initial stage. As the time elapses, larger PCM latent heat produces higher discharging rate of the LHTES unit. It is specific that the discharging rate climbs from 115.122 to 257.603 W when the PCM latent heat rises from 100 to 250 kJ/kg. The PCM latent heat is critical to discharging performance of the LHTES unit. Fig. 11 (d) reveals that the total discharging energy increases with augment of the PCM latent heat. The difference among these LHTES unit enlarges as time elapses. The discharging energy is achieved as approximately 660.362, 783.635, 918.373 and 974.153 kJ for the PCM latent heat cases of 100–250 kJ/kg at 200 min. It is observed in Fig. 11 (e) and (f) that the solidification zone reduces with augment of the PCM latent heat, in spite of the total discharging energy is improved under the large PCM latent heat condition. This phenomenon is attributed to fact that PCM with larger latent heat is capable of storing more thermal energy.

4. Conclusions

This paper introduces a PID controller into a LHTES unit to regulate the discharging performance. The outlet water temperature can be precisely controlled by means of the inlet velocity variation. A theoretical model is built based on coupling of phase change heat transfer with the PID control. Experimental results are used to validate the proposed theoretical model. Parameters of the PID controller are firstly optimized and it is found that K_p, K_i and K_d have obvious effects on

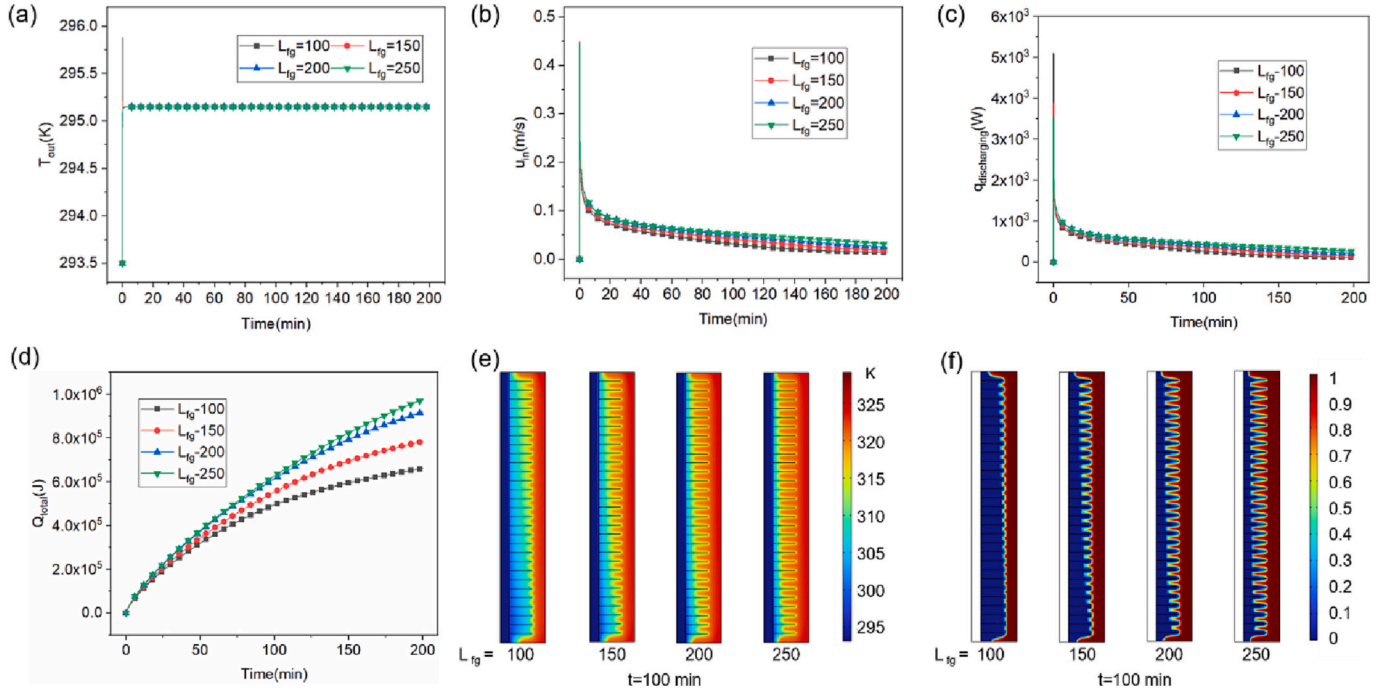

Fig. 11. Transient discharging performance of the LHTES system with various PCM latent heat. (a) Outlet water temperature, (b) Outlet water flow rate, (c) Discharging rate, (d) Total discharging energy, (e) Temperature contour and (f) Phase change contour.

performance of the PID controller. K_p of −0.02 m/(s·K), K_i of −0.15 m/(s^2·K) and K_d of −0.001 m/K are picked out according to dynamic regulation of the outlet water temperature. The coupled unit can adjust the inlet water velocity to ensure the transient outlet water temperature exactly match with target.

System parameters including target outlet temperature and thermophysical properties of PCM are analyzed in this investigation. Related results indicate that higher target temperature produces larger heat discharging rate and reduces the outlet water flow rate accordingly. Lower target outlet temperature means less heat transfer temperature difference between PCM and water, which then results in larger discharging rate. The discharging rate of the LHTES unit decreases gradually to 257.691, 233.894, 217.419 and 208.572 W at 200 min. The total discharging energy reduces with augment of the target outlet temperature. The water velocity, discharging rate and total discharging energy increase as the PCM melting point rises. It is specific that the total discharging energy is 775.515, 885.508, 954.005 and 1060.105 kJ for the LHTES units containing PCM with melting points of 315.15–327.15 K. Larger PCM thermal conductivity contributes to higher water velocity, discharging rate and total discharging energy. The discharging rate at 200 min can climb to 294.437 W at the PCM thermal conductivity of 0.8 W/(m·K). Temperature distribution tends to be more uniformed in the LHTES unit with larger PCM thermal conductivity. The PCM latent heat is a critical parameter to discharging performance of the LHTES system. Larger PCM thermal conductivity enables to improve the water velocity, discharging rate and total discharging energy. When PCM latent heat rises to 250 kJ/kg, the discharging rate and total discharging energy respectively increase to 257.603 W and 974.153 kJ at 200 min.

In conclusion, the built coupling system possesses flexible discharging performance and could exhibit substantial potentials in promotion and application of LHTES technology.

CRediT authorship contribution statement

Zhaoli Zhang: Conceptualization, Methodology, Writing - Original draft preparation. **Jiayu Liu**: Data curation, Writing & Editing. **Nan Zhang**: Writing - Review & Editing, Visualization. **Xiaoling Cao**: Review & Editing, Visualization. **Yanping Yuan**: Resources, Writing - Review & Editing, Supervision. **Muhammad Sultan**: Writing - Review & Editing, Visualization. **Shady Attia**: Writing - Review & Editing, Supervision.

Declaration of competing interest

The authors declare that they have no known competing financial interests or personal relationships that could have appeared to influence the work reported in this paper.

Data availability

Data will be made available on request.

Acknowledgements

This work was supported by the National Natural Science Foundation of China (No. 52108077 and 52006183), Natural Science Foundation of Sichuan Province (No. 23NSFSC4267).

References

[1] A. Hussain, S.M. Arif, M. Aslam, Emerging renewable and sustainable energy technologies: state of the art, Renew. Sust. Energ. Rev. 71 (2017) 12–28.
[2] J. Nowotny, J. Dodson, S. Fiechter, T.M. Gür, B. Kennedy, W. Macyk, T. Bak, W. Sigmund, M. Yamawaki, K.A. Rahman, Towards global sustainability: education on environmentally clean energy technologies, Renew. Sust. Energ. Rev. 81 (2018) 2541–2551.
[3] N.M.A. Huijts, E.J.E. Molin, L. Steg, Psychological factors influencing sustainable energy technology acceptance: a review-based comprehensive framework, Renew. Sust. Energ. Rev. 16 (2012) 525–531.
[4] W. Van der Gaast, K. Begg, A. Flamos, Promoting sustainable energy technology transfers to developing countries through the CDM, Appl. Energy 86 (2009) 230–236.
[5] G. Alva, Y. Lin, G. Fang, An overview of thermal energy storage systems, Energy 144 (2018) 341–378.
[6] F. Liu, G. Zhang, Study on melting and solidification performances improvement of phase change material using novel branch fin structure, J. Energy Storage 63 (2023), 107097.
[7] F. Agyenim, N. Hewitt, P. Eames, M. Smyth, A review of materials, heat transfer and phase change problem formulation for latent heat thermal energy storage systems (LHTESS), Renew. Sust. Energ. Rev. 14 (2010) 615–628.
[8] Y. Gao, X. Meng, A comprehensive review of integrating phase change materials in building bricks: methods, performance and applications, J. Energy Storage 62 (2023), 106913.
[9] A. Awasthi, Y. Jeon, Detailed numerical analysis of heat transfer enhancement in horizontal shell-and-tube-type n-eicosane-based latent thermal energy storage system, J. Energy Storage 63 (2023), 106994.
[10] M. Sheikholeslami, Efficacy of porous foam on discharging of phase change material with inclusion of hybrid nanomaterial, J. Energy Storage 62 (2023), 106925.
[11] S.R.L. da Cunha, J.L.B. de Aguiar, Phase change materials and energy efficiency of buildings: a review of knowledge, J. Energy Storage 27 (2020), https://doi.org/10.1016/j.est.2019.101083.
[12] F. Selimefendigil, H.F. Öztop, Effects of flow separation and shape factor of nanoparticles in heat transfer fluid for convection thorough phase change material (PCM) installed cylinder for energy technology applications, J. Energy Storage 41 (2021), 102945.
[13] U. Berardi, S. Soudian, Experimental investigation of latent heat thermal energy storage using PCMs with different melting temperatures for building retrofit, Energy Build. 185 (2019) 180–195.
[14] D.G. Atinafu, S. Wi, B.Y. Yun, S. Kim, Engineering biochar with multiwalled carbon nanotube for efficient phase change material encapsulation and thermal energy storage, Energy 216 (2021), 119294.
[15] S. Ishak, S. Mandal, H.-S. Lee, J.K. Singh, Effect of core-shell ratio on the thermal energy storage capacity of SiO_2 encapsulated lauric acid, J. Energy Storage 42 (2021), 103029.
[16] X. Guo, H. Wei, X. He, M. He, D. Yang, Integrating phase change material in building envelopes combined with the earth-to-air heat exchanger for indoor thermal environment regulation, Build. Environ. 221 (2022), 109318, https://doi.org/10.1016/j.buildenv.2022.109318.
[17] K. Hosseinzadeh, M.A.E. Moghaddam, A. Asadi, A.R. Mogharrebi, D.D. Ganji, Effect of internal fins along with hybrid nano-particles on solid process in star shape triplex latent heat thermal energy storage system by numerical simulation, Renew. Energy 154 (2020) 497–507.
[18] J. Lei, Y. Tian, D. Zhou, W. Ye, Y. Huang, Y. Zhang, Heat transfer enhancement in latent heat thermal energy storage using copper foams with varying porosity, Sol. Energy 221 (2021) 75–86.
[19] X. Liu, H. Wang, Q. Xu, Q. Luo, Y. Song, Y. Tian, M. Chen, Y. Xuan, Y. Jin, Y. Jia, High thermal conductivity and high energy density compatible latent heat thermal energy storage enabled by porous AlN ceramics composites, Int. J. Heat Mass Transf. 175 (2021), 121405.
[20] I. Baskar, M. Chellapandian, Experimental and finite element analysis on the developed real-time form stable PCM based roof system for thermal energy storage applications, Energy Build. 276 (2022), 112514.
[21] P. Cheng, X. Chen, H. Gao, X. Zhang, Z. Tang, A. Li, G. Wang, Different dimensional nanoadditives for thermal conductivity enhancement of phase change materials: fundamentals and applications, Nano Energy 85 (2021), 105948.
[22] S. Deng, C. Nie, G. Wei, W.-B. Ye, Improving the melting performance of a horizontal shell-tube latent-heat thermal energy storage unit using local enhanced finned tube, Energy Build. 183 (2019) 161–173.
[23] Y. Su, Q. Yu, L. Zeng, Parameter self-tuning pid control for greenhouse climate control problem, IEEE Access 8 (2020) 186157–186171.
[24] M.N. Ajour, M.J. Abduaal, F.A. Hariri, N.H. Abu-Hamdeh, S.M. Sajadi, Approving a new PID controller and using PCM to intensify electricity generation in a green building, Sustain. Energy Technol. Assessments 53 (2022), 102393.
[25] S.M. Alghamdi, M.N. Ajour, N.H. Abu-Hamdeh, A. Karimipour, Introducing a new PID controller to control the addition of PCM to the building with ventilation heat recovery installation to reduce the energy demand of the cooling system, J. Build. Eng. 56 (2022), 104766.
[26] C. Piao, W. Wang, Z. Liu, C. Wu, R. Yuan, Research on vehicle cabin temperature and thermal comfort optimal control based on fuzzy PID, in: J. Phys. Conf. Ser., IOP Publishing, 2021, p. 32039.
[27] H. Ma, Y. Xie, K. Duan, X. Song, R. Ding, C. Hou, Dynamic control method of flue gas heat transfer system in the waste heat recovery process, Energy 259 (2022), 125010.
[28] M. Huo, Z. Wu, T. He, D. Li, Thermodynamic modeling and control of hybrid solar-fossil fuel power generation and storage system, Appl. Therm. Eng. 229 (2023), 120593, https://doi.org/10.1016/j.applthermaleng.2023.120593.
[29] P. Singh, R.K. Sharma, M. Khalid, R. Goyal, A. Sarı, V.V. Tyagi, Evaluation of carbon based-supporting materials for developing form-stable organic phase change materials for thermal energy storage: a review, Sol. Energy Mater. Sol. Cells 246 (2022), 111896.

[30] D. Das, U. Bordoloi, H.H. Muigai, P. Kalita, A novel form stable PCM based bio composite material for solar thermal energy storage applications, J. Energy Storage 30 (2020), 101403.
[31] X.Y.D. Soo, Z.M. Png, M.H. Chua, J.C.C. Yeo, P.J. Ong, S. Wang, X. Wang, A. Suwardi, J. Cao, Y. Chen, A highly flexible form-stable silicone-octadecane PCM composite for heat harvesting, Mater. Today Adv. 14 (2022), 100227.
[32] B. Gürel, Thermal performance evaluation for solidification process of latent heat thermal energy storage in a corrugated plate heat exchanger, Appl. Therm. Eng. 174 (2020), 115312.
[33] B. Gürel, A numerical investigation of the melting heat transfer characteristics of phase change materials in different plate heat exchanger (latent heat thermal energy storage) systems, Int. J. Heat Mass Transf. 148 (2020), 119117.